Localization of the Extracellular End of the Voltage Sensor S4 in a Potassium Channel

Fredrik Elinder, Peter Århem, and H. Peter Larsson
The Nobel Institute for Neurophysiology, Department of Neuroscience, Karolinska Institutet, SE-171 77 Stockholm, Sweden

ABSTRACT The opening and closing of the pore of voltage-gated ion channels is the basis for the nervous impulse. These conformational changes are triggered by the movement of an intrinsic voltage sensor, the fourth transmembrane segment, S4. The central problem of how the movement of S4 is coupled to channel opening and where S4 is located in relation to the pore is still unsolved. Here, we estimate the position of the extracellular end of S4 in the *Shaker* potassium channel by analyzing the electrostatic effect of introduced charges in the pore-forming motif (S5–S6). We also present a three-dimensional model for all transmembrane segments. Knowledge of this structure is essential for the attempts to understand how voltage opens these channels.

INTRODUCTION

Voltage-gated ion channels are key elements in the generation of the nervous impulse. They consist of an ion-selective pore, several activation and inactivation gates, and a voltage-sensing machinery (Hille, 1992). The recently solved structure of the bacterial KcsA channel most likely provides a good model of the central, pore-containing part of voltage-gated potassium channels, including the gates (Doyle et al., 1998; Yellen, 1998). The positively-charged fourth transmembrane segment (S4) has been identified as voltage sensor (Mannuzzu et al., 1996; Larsson et al., 1996; Seoh et al., 1996; Aggarwal and MacKinnon, 1996; Yusaf et al., 1996), but its location in relation to the pore is not known. The purpose of the present study is to obtain information about this location. Our strategy is to use the structure of the KcsA channel as a model for the pore region of the *Shaker* potassium channel and to measure the effects of introduced charges in different positions in this region of the *Shaker* potassium channel.

Altering the charge of a surface amino acid will alter the electric field sensed by the voltage sensor and, hence, shift the voltage-dependent parameters of the ion channel along the voltage axis (McLaughlin, 1989; Hille, 1992). These shifts should be larger the closer the introduced charge is to the moving, charged parts of the protein. In the latter part of the paper, we will interpret these shifts as caused by interactions with the extracellular end of the voltage sensor S4 and translate these shifts into geometrical distances to this part of S4. We introduce a cysteine at different positions in a non-inactivating N-terminal deleted *Shaker* potassium channel (ShH4IR) and express these channels in *Xenopus* oocytes. This allows us to add a negative or a positive charge to the specific positions in situ by modifying the introduced cysteines with differently-charged reagents ($MTSES^-$ or $MTSET^+$, see Materials and Methods). We selected four extracellular residues that cover most of the circumference of the pore-forming part of the channel (Fig. 1): one at the extracellular end of S5 (A419) which has been suggested to be close to S4 (Elinder and Århem, 1999), two at the extracellular end of S6 (V451 and G452) which are involved in slow inactivation (Larsson and Elinder, 2000), and one at the extracellular end of the pore helix (P430). The results suggest that the extracellular end of S4 is located close to the extracellular end of S5.

Received for publication 11 September 2000 and in final form 23 January 2001.

Address reprint requests to Peter Århem, The Nobel Institute for Neurophysiology, Dept. of Neuroscience, Berzelius väg 3, Karolinska Institutet, S-171 77 Stockholm, Sweden. Tel.: +46-8-728-69-03; Fax: +46-8-34-95-44; E-mail: peter.arhem@neuro.ki.se.

0006-3495/01/04/1802/08 $2.00

MATERIALS AND METHODS

Molecular biology

The experiments were performed on *Shaker* H4 channels (Kamb et al., 1987), made incapable of fast-inactivation by the Δ6-46 deletion (Hoshi et al., 1990). Cysteines were substituted using the QuikChange Kit (Stratagene, La Jolla, CA). cRNA was transcribed using the T7 mMessage mMachine kit (Ambion Inc., Austin, TX) and injected in *Xenopus laevis* oocytes (20–5000 pg/cell) using a Nanoject injector (Drummond Scientific Co., Broomall, PA). The oocytes were maintained at 12°C in a modified Barth's solution (MBS, in mM: 88 NaCl, 1 KCl, 2.4 $NaHCO_3$, 15 HEPES, 0.33 $Ca(NO_3)_2$, 0.41 $CaCl_2$, and 0.82 $MgSO_4$) adjusted to pH 7.5 by NaOH, and supplemented with penicillin (10 μg/ml) and streptomycin (10 μg/ml). The electrophysiological experiments were made 2–20 days after injection of mRNA.

Electrophysiology, solutions, and reagents

The currents were measured with the two-electrode voltage-clamp technique (CA-1 amplifier, Dagan Corporation, Minneapolis, MN). Microelectrodes were made from borosilicate glass and filled with a 3M KCl solution. The resulting resistance varied between 0.5 and 2.0 MΩ. The amplifier's capacitance and leak compensation were used, and the currents were low-pass filtered at 1 kHz. All experiments were carried out at room temperature (20–23°C). For the electrophysiological experiments, we used the MBS solution described above. To screen surface charges, we added 20 mM $MgCl_2$ to the MBS solution. Mg^{2+} ions have been shown to shift voltage-dependent parameters equally and, therefore, have been suggested to exert pure screening of surface charges without directly binding to potassium channels (Elinder and Århem, 1998; Elinder et al., 1998). To

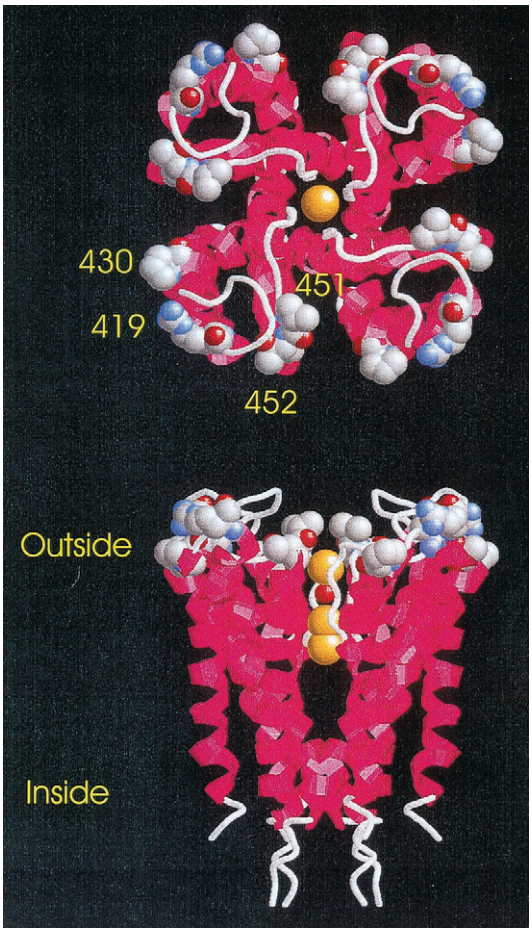

FIGURE 1 Positions of the modified residues. Top view (*upper part*) and side view (*lower part*) of the bacterial KcsA channel (only backbone is shown). Mutations used in the present investigation (space filled residues; *gray* = C, *red* = O; *blue* = N) are labeled. A419 (at the extracellular end of S5), P430 (at the extracellular end of the pore helix), and, V451 and G452 (at the extracellular end of S6) in *Shaker* corresponds to R52, P63, V84, and T85 in KscA. In the center of the channel, three potassium ions (*yellow*) and one water molecule (*red*) are shown in the selectivity filter.

alter the charge at the substituted cysteines, the membrane-impermeant thiol reagents, positively-charged MTSET ([2-(trimethylammonium)ethyl-]methanethiosulfonate, bromide) and negatively-charged MTSES (sodium (2-sulfonatoethyl)methanethiosulfonate) (Toronto Research Chemicals Inc., North York, Ontario, Canada), were applied continuously in the bath solution by a gravity-driven perfusion system, and the modification was assayed functionally in two-electrode voltage-clamped oocytes, as described earlier (Larsson et al., 1996; Baker et al., 1998). The cysteine reagents were applied to saturation (typically 100 μM MTSET or 1 mM MTSES for 200 s). The molecular structures of the attached reagents are shown in Fig. 2. The sizes are close to that of the positively charged amino acid residue arginine.

Shift measurements

The steady-state potassium conductance $G_{K(V)}$ was calculated as

$$G_K(V) = I_K(V)/(V - E_K), \qquad (1)$$

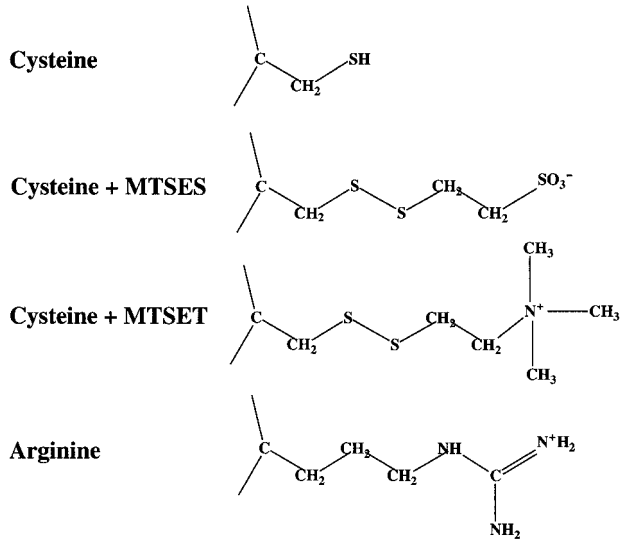

FIGURE 2 Schematic structures of cysteine residues without and with attached MTS reagents. For comparison, a positively charged arginine residue is shown. The residue in KcsA corresponding to 419A in *Shaker* is an arginine (see Fig. 1).

where $I_K(V)$ is the steady-state current, V is the membrane potential measured in the bulk solutions, and E_K is the equilibrium potential (−80 mV). For 419C, 451C, and 452C, the shifts of the $G(V)$ curves caused by either MTS reagents or Mg^{2+} were measured by sliding the control $G(V)$ to overlap (most importantly the lower part of the curves, because the curves were not normalized) the Mg^{2+} or MTS $G(V)$. For 430C, we had to normalize the maximum conductance (at ~+60 mV) before sliding the $G(V)$ curves.

Calculation of the surface potential

The change in the surface potential caused by the cysteine reagents was estimated directly from the voltage shift of the $G(V)$ curve (ΔV_{MTS}). To minimize the errors in our calculations caused by possible nonelectrostatic effects of the MTS reagents, we calculated the change in surface potential, $\Delta\psi$, as $(\Delta V_{MTSET} - \Delta V_{MTSES})/2$. To confirm that this shift was caused by a change in the surface charge density and consequently in the surface potential, we measured the voltage shift of the $G(V)$ curve induced by an extracellular application of 20 mM Mg^{2+} (ΔV_{Mg}) and used the Grahame equation (Grahame, 1947) for a quantitative evaluation:

$$\sigma^2 = 2\varepsilon_r\varepsilon_0 RT \sum_i c_i[\exp(-z_i F\psi R^{-1}T^{-1}) - 1], \qquad (2)$$

where σ is the surface charge density, ϵ_r is the dielectric constant of the medium (80 in water), ϵ_0 is the permittivity of free space ($8.85 \cdot 10^{-12}$ F·m^{-1}), c_i is the bulk concentration, and z_i is the valence of the ith ionic species in the extracellular solution. ψ is the surface potential. R, T, and F have their usual thermodynamic significance. To relate the Mg-induced shift, ΔV_{Mg}, to the surface potential, ψ, Eq. 2 has to be solved numerically. In brief, one has to find the (constant) σ value that, for the two different Mg^{2+} concentrations (c_{Mg2+}), will give two values of ψ that differ by ΔV_{Mg} (see pp 457–470 in Hille (1992) for more detailed explanations of surface charge calculations). The final concentrations of the different valencies that were used in the calculations were (in mM, note that approximately 10 mM NaOH was added for the pH adjustment) 100 cation$^+$, 1.6 cation^{2+}, 93 anion$^-$, and 0.8 anion^{2-}. Although Eq. 2 is

strictly valid only for a uniformly smeared charge, it has been shown that the equation can be used as an approximation for charge densities more negative than −0.16 elementary charges per nm^2 (Peitzsch et al., 1995). The surface charge density of the *Shaker* potassium channel has previously been estimated to be $-0.27e$ nm^{-2} (Elinder et al., 1998). Using Eq. 2, we calculated the predictions of the changes in the Mg^{2+}-induced shifts ($\Delta\Delta V_{Mg}$ in Table 1) from the measured shifts induced by the MTS-reagents ($\Delta\psi$ in Table 1) and the Mg^{2+}-induced shifts of the unmodified channels (ΔV_{Mg} in Table 1).

Estimation of the S4 location

The potential ψ_r, at a distance r, from an elementary charge e located at the border between a low-dielectric (membrane) and a high-dielectric (water) medium is (McLaughlin, 1989; Elinder and Århem, 1999)

$$\psi_r = 2e \exp(-\kappa r)/(4\pi\varepsilon_0\varepsilon_r r), \quad (3)$$

where κ is the inverse of the Debye length in the aqueous phase (9.6 Å in the MBS solution, see Elinder and Århem (1999) for calculation). Because *Shaker* is a homotetramer and we changed the charge of a residue in all four subunits, Eq. 3 is modified to calculate the predicted change in potential at a specific position (x, y) in the surface plane of the channel

$$\Delta\psi_{pred}(x, y) = \sum_{i=1}^{4} \frac{2e \exp(-\kappa r(x - x_i, y - y_i))}{4\pi\varepsilon_0\varepsilon_r r(x - x_i, y - y_i)}, \quad (4)$$

where (x_i, y_i) is the position of a surface charge residue in the ith subunit. Assuming a helical screw motion of S4, we can estimate the location of the extracellular end of S4 with no deeper knowledge of the interior of the protein (see the Results section). We assume that the four S4s are symmetrically located in the channel. To determine the position of the extracellular end of S4, we compared the experimentally obtained change in surface potential ($\Delta\psi$) with the predicted value from Eq. 4 by

$$\text{r.m.s.} \quad \Delta\Delta\psi(x, y) = \left(\left(\sum_{n=1}^{4} (\Delta\psi_{n,pred}(x, y) - \Delta\psi_n)^2\right)/4\right)^{1/2}, \quad (5)$$

where n indicates the identity of the mutation (a total of four in the present study). The r.m.s. values were determined for an area of 100 × 100 Å^2 at every 2 × 2 Å^2 (see Fig. 5). The extracellular end of S4 is most likely to be found at the position where the r.m.s. $\Delta\Delta\psi$ has its smallest value.

RESULTS

$MTSET^+$ and $MTSES^-$ shift the $G(V)$ of 419C in opposite directions

Figure 3 *A* shows the effect of differently-charged cysteine reagents on 419C channels. $MTSES^-$ shifted the conductance versus voltage curve $G(V)$ in the negative direction along the voltage axis on average −10.2 mV (Table 1). $MTSET^+$ shifted the $G(V)$ in the positive direction on average +6.1 mV (Table 1). The amplitude of the maximum conductance was only marginally affected (<5%). The shifts caused by $MTSES^-$ and $MTSET^+$ are in opposite directions but not perfectly symmetrical, suggesting that the structure of the MTS-reagent itself slightly affects the stability of the channel in some of its conformational states. To separate the $G(V)$ shifts caused by electrostatic effects ($\Delta\psi$) from nonelectrostatic effects of the MTS reagents, we assumed that the nonelectrostatic effects were the same for the

TABLE 1 Effects of mutations, MTS-reagents, and Mg^{2+} on $G(V)$ curves

	$V_{1/2}$ (mV)	ΔV_{MTS} (mV)	$\Delta\psi$ (mV)	ΔV_{Mg} (mV)	$\Delta\Delta V_{Mg}$ (mV)	
					Experiment	Prediction
WT	−23.7 ± 2.2 (13)		−0.1	+13.4 ± 0.3 (11)		
WT + $MTSES^-$	−23.9 ± 1.7 (4)	+0.1 ± 0.3 (4)		+13.4 ± 0.8 (4)	−0.2 ± 0.4 (3)	−0.0
WT + $MTSET^+$	−24.1 ± 2.8 (5)	−0.1 ± 0.6 (5)		+13.8 ± 0.5 (5)	−0.1 ± 0.1 (5)	+0.0
A419C	−24.5 ± 1.0 (8)		+8.2	+13.8 ± 0.5 (13)		
A419C + $MTSES^-$	−35.5 ± 1.5 (2)	−10.2 ± 0.9 (6)**		+16.1 ± 0.9 (5)	+1.9 ± 0.6 (5)*	+2.3
A419C + $MTSET^+$	−17.2 ± 3.4 (3)	+6.1 ± 0.8 (6)**		+11.7 ± 1.0 (6)	−2.0 ± 0.4 (5)**	−2.3
P430C	−22.4 ± 1.0 (19)		+3.8	+13.2 ± 0.5 (16)		
P430C + $MTSES^-$	−5.4 ± 2.1 (7)	+19.1 ± 1.9 (7)**		+13.5 ± 1.1 (4)	−1.0 ± 0.6 (3)	+1.1
P430C + $MTSET^+$	+2.7 ± 2.6 (3)	+26.7 ± 0.9 (3)**		n.d.	n.d.	−1.1
V451C	−23.0 ± 0.9 (6)		+3.6	+13.3 ± 0.4 (6)		
V451C + $MTSES^-$	−26.2 ± 0.8 (3)	−3.5 ± 0.3 (3)*		+14.8 ± 0.7 (3)	+1.5 ± 0.3 (3)*	+1.0
V451C + $MTSET^+$	−19.7 ± 2.3 (3)	+3.7 ± 0.7 (3)*		+12.5 ± 0.8 (3)	−0.5 ± 0.3 (3)	−1.0
G452C	−24.3 ± 1.1 (10)		+5.6	+11.9 ± 0.7 (10)		
G452C + $MTSES^-$	−29.0 ± 1.7 (3)	−4.0 ± 0.3 (3)**		+14.5 ± 1.8 (3)	+1.7 ± 0.3 (3)*	+1.5
G452C + $MTSET^+$	−17.0 ± 1.9 (6)	+7.3 ± 0.7 (6)**		+9.8 ± 0.9 (5)	−1.2 ± 0.4 (5)*	−1.5

$V_{1/2}$ is the mid-point potential of the $G(V)$ curve. ΔV_{MTS} is the MTS-induced shift of the $G(V)$ curve measured for each individual oocyte. $\Delta\psi$ is the electrostatic effect of the MTS reagents on the $G(V)$ curves and is calculated as $(\Delta V_{MTSET} - \Delta V_{MTSES})/2$. ΔV_{Mg} is the Mg^{2+} (20 mM)-induced shift of the $G(V)$. $\Delta\Delta V_{Mg}$ is the MTS-induced change in ΔV_{Mg} (i.e., ΔV_{Mg} [after MTS application] − ΔV_{Mg} [before MTS application]) for each individual oocyte. Predictions are calculated as described in Materials and Methods.

Values given as mean ± SEM (n). That ΔV_{MTS} and $\Delta\Delta V_{Mg}$ of the mutations were significantly different from WT was evaluated with a paired t test: *($p < 0.05$); **($p < 0.01$).

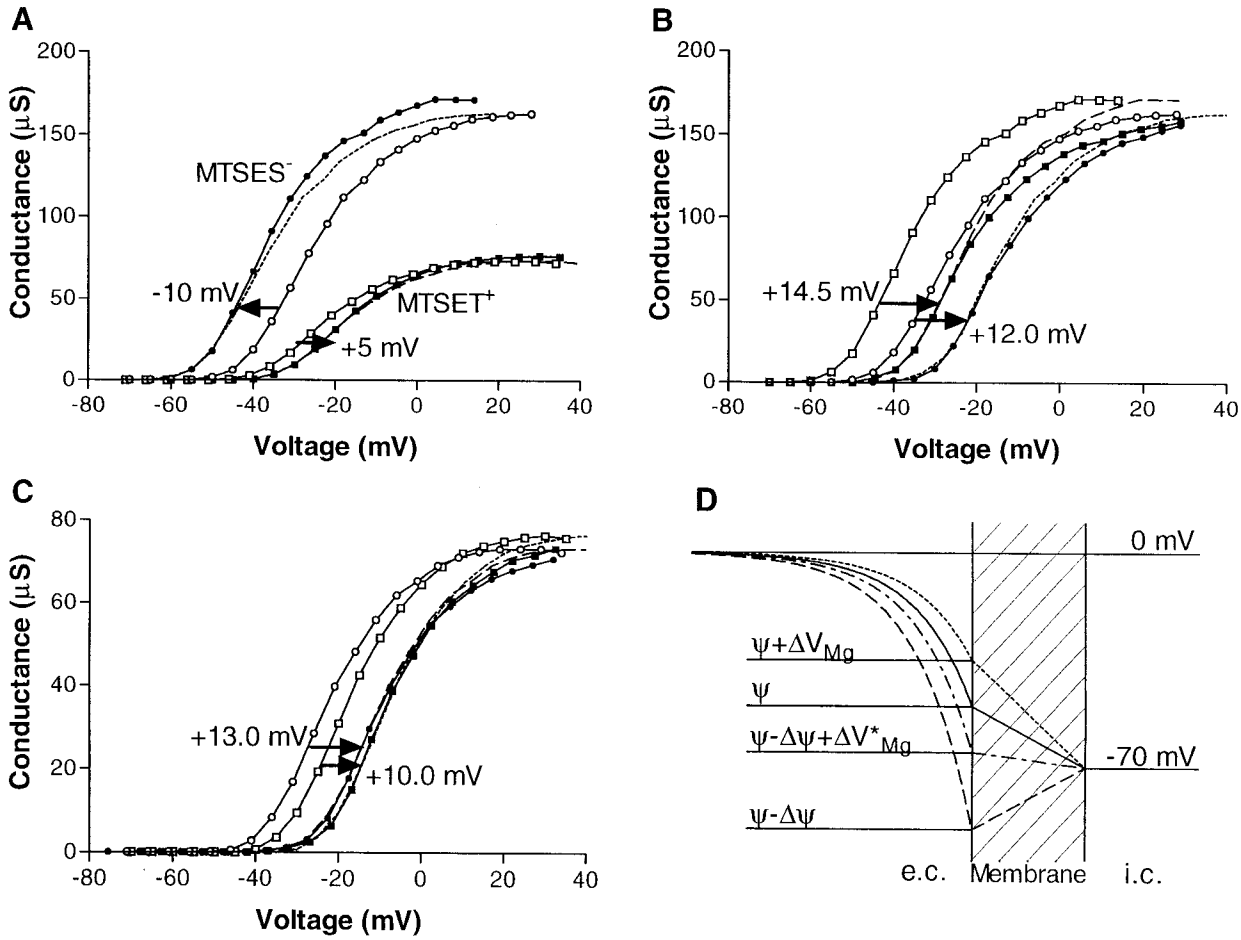

FIGURE 3 Effects of charged cysteine reagents and Mg^{2+} on the $G(V)$ curve of A419C. (*A*) $G(V)$ curves of 419C channels before (○ and □) and after $MTSET^+$ (■) or $MTSES^-$ (●) treatment. The negatively-charged $MTSES^-$ shifts the $G(V)$ in the negative direction, and the positively-charged $MTSET^+$ shifts the $G(V)$ in the positive direction. The dotted lines are the control data shifted as indicated. Note that the data are from two different cells. (*B*) $G(V)$ curves of 419C channels (○) and $MTSES^-$-modified 419C channels (□) in MBS solution (*open symbols*) and in MBS + 20 mM Mg^{2+} (*filled symbols*). 20 mM Mg^{2+} shifts the control $G(V)$ less than the $G(V)$ of the $MTSES^+$-treated channels. (*C*) $G(V)$ curves of 419C channels (○) and $MTSET^+$-modified 419C channels (□) in MBS solution (*open symbols*) and in MBS + 20 mM Mg^{2+} (*filled symbols*). 20 mM Mg^{2+} shifts the control $G(V)$ more than the $G(V)$ of the $MTSET^+$-treated channels. (*D*) Schematic figure showing the effects of a negative surface potential and changes in the surface potential on the electric field. The extracellular (*e.c.*) potential far from the membrane is 0 mV and the intracellular (*i.c.*) potential is set to −70 mV. The potential approaches the negative surface potential (ψ) as one is approaching the channel/membrane that has a net negative surface charge. Modification of an extracellularly-exposed cysteine with $MTSES^-$ makes the surface charge density more negative, and, consequently, the surface potential becomes more negative (by $-\Delta\psi$). 20 mM Mg^{2+} (incompletely) screens the surface charges and changes the surface potential by ΔV_{Mg} (control channels) or ΔV^*_{Mg} ($MTSES^-$-modified channels). Note that $\Delta V^*_{Mg} > \Delta V_{Mg}$.

two MTS reagents and that the difference between the $MTSET^+$-induced and the $MTSES^-$-induced shifts is equal to $2\Delta\psi$. This gave $\Delta\psi = (+6.1 - (-10.2))/2 = 8.2$ mV. To verify that this value was due to electrostatic interactions and reflected a change in surface potential, we analyzed the effects of Mg^{2+} on the $G(V)$ curves.

The $\Delta\psi$ component of the $G(V)$ shifts are due to electrostatic interactions

According to the surface charge theory, raising the external concentration of divalent cations will screen the exposed surface charges and reduce the absolute value of the (negative) surface potential (McLaughlin, 1989; Hille, 1992) (see Fig. 3 *D*). This reduction in surface potential will lead to a shift of the voltage-dependent parameters along the voltage axis, which is roughly proportional to the absolute value of the surface potential. Therefore, to test if we have altered the surface charge density and consequently the surface potential by the introduced charged MTS reagents, we perfused the channels with an extracellular solution containing an increased concentration of $MgCl_2$ (the Cl^- ions having negligible effects according to Eq. 2).

The application of 20 mM Mg^{2+} shifted the $G(V)$ curve (ΔV_{Mg}) for 419C channels in the positive direction along the voltage axis (Fig. 3, *B* and *C*) on average +13.8 mV (Table

1). ΔV_{Mg} increased to 16.1 mV (Table 1) when 419C channels were modified with $MTSES^-$ (Fig. 3 *B*) and decreased to 11.7 mV (Table 1) when 419C channels were modified with $MTSET^+$ (Fig. 3 *C*). These results are qualitatively what is expected from a change in surface potential by the MTS-modifications of 419C. To make a quantitative evaluation, we used Eq. 2 to calculate the predicted ΔV_{Mg} for the MTS-modified channels based on the ΔV_{Mg} for the unmodified channels (+13.8 mV) and on the $\Delta\psi$ of the MTS-modified channels (8.2 mV). The predicted shifts were +16.1 mV and +11.5 mV, for $MTSES^-$- and $MTSET^+$-modified channels respectively, which are in agreement with the experimentally found shifts showing that $\Delta\psi$ is of electrostatic origin.

Electrostatic effects of other residues

We have shown that a charge at residue 419 in a *Shaker* potassium channel affects the voltage sensing of the channel with ±8.2 mV, the sign depending on the sign of the charge. With the same method we could also show that a charge at residue 451 affects the voltage sensing of the channel with ±3.6 mV and a charge at residue 452 affects the voltage sensing of the channel with ±5.6 mV (Table 1). The effect of the MTS-modification of residue 430C deviated from those of the other residues. First, the MTS reagents reduced the maximum conductance considerably: $MTSES^-$ by 67 ± 11% (mean ± SD, $n = 7$), and $MTSET^+$ by 81 ± 12% (mean ± SD, $n = 5$). Second, the MTS-induced shifts were both in the positive direction: +19.1 mV for $MTSES^-$ and +26.7 mV for $MTSET^+$ (Table 1). This suggests that the MTS molecules have a major nonelectrostatic effect on the $G(V)$ curve in addition to a minor electrostatic effect: a +22.9 mV shift caused by nonelectrostatic effects and a ±3.8 mV shift by electrostatic effects. The ΔV_{Mg} of 430C was not significantly altered by $MTSES^-$ (Table 1). This suggests that residue 430 contributes very little, or not at all, to the surface potential felt by the voltage sensor. In the following calculation, we used the $\Delta\psi$ values as the estimate of the electrostatic effect of the introduced charges (for position 430, see also Appendix).

The location of S4

One simple interpretation of our results is that, of the residues studied, residue 419 should be located closest to the voltage sensor S4, whereas residue 452 is located further away from S4, and residues 430 and 451 are located even further from S4. This suggests that S4 is located close to S5 (see Fig. 1). The exact effect of the introduced surface charges on the voltage dependence of the channel depends on the exact movement of all the charged residues of the channel in relation to the introduced charge. In the following quantitative analysis, we will assume that it is mainly the charges in S4 that are moving and that all other charges are relatively immobile. In addition, to make a quantitative estimation of the position of S4, we have to make some assumptions about the structure and the movement of S4.

The S4 segment is most likely an α-helix (Yang et al., 1997; Cha et al., 1999; Glauner et al., 1999; Li-Smerin et al., 2000a), which would make the charges on S4 wrap around this helix like a helical screw (Catterall, 1986). The movement of S4 during the opening of the channel exposes three charged residues into the extracellular solution (Baker et al., 1998; Tiwari-Woodruff et al., 2000), probably reflecting three consecutive activation steps (Keynes and Elinder, 1999). If we assume that the S4 motion is that of a helical screw moving in three steps (Catterall, 1986; Keynes and Elinder, 1999), then this motion is electrostatically equivalent to moving the three bottom charges from the cytosol to the extracellular solution while keeping the charges inside the protein fixed (Fig. 4). Thus, even though the electrical potential caused by an extracellular surface charge is not negligible in the membrane, it does not affect the gating because the intramembranous charge pattern is unaltered during gating in this model. Furthermore, the electrical potential caused by an extracellular surface charge is negligible at the intracellular side of the membrane (see Fig. 5 in Mathias et al., 1992). For the following quantitative analysis, we used this helical-screw model of S4 motion. In this model, it is only the electrical potential at the extracellular surface where the three top S4 charges (R362, R365, and R368) emerge, that determines the size of the $G(V)$ shift caused by changes of the extracellular surface charges. The

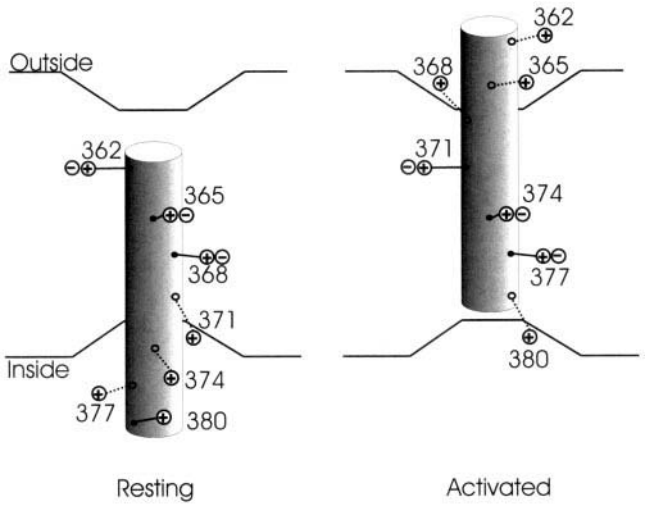

FIGURE 4 Schematic model of S4 movement. Positions of S4 in resting and activated states. Dotted side chains indicate that the α-carbons of the positively charged residues on S4 are located on the back of the helical core. Note that the charge pattern in the membrane does not change upon activation. The three charged extracellular residues in the activated position are located on one side of the helical core. The labels indicate the residue numbers of the S4 charges in *Shaker*.

three top charges on S4 would all lie on the same side of an α-helix (Fig. 4) and we have, in the following approximate calculation, treated them as a point charge (for quantitative justifications see Appendix).

We used Eq. 4 to predict the surface potential at different positions $\Delta\psi_{pred}(x, y)$ caused by the introduction of a charged residue in all four subunits. We calculated the differences between our experimental data, $\Delta\psi$, and the predicted values $\Delta\psi_{pred}(x, y)$ for all possible positions (x, y) of the top charges of S4 on the channel surface (see Materials and Methods). The smaller the difference is for a certain position of S4, the higher the probability that S4 is located at that position. Fig. 5 *A* shows the r.m.s. values of these differences calculated for the entire channel surface. The resulting landscape shows four distinct valleys (*red*) at a distance of ~11 Å outside the center of the extracellular end of S5. These valleys suggest, under the assumption of the helical-screw model above, the location of the top charges of S4. The low error value at the minimum (0.77 mV) indicates that it is a good fit to our data.

DISCUSSION

We have tested the effect of an introduced charge at different positions in the extracellular end of the pore domain of *Shaker* potassium channels. The key finding was that a charge in S5 (residue 419) electrostatically affects the voltage sensor more than a charge at other positions. Assuming that the electrostatic effects are with the charges in S4, this suggests that S4 is located close to S5. We also made a quantitative estimation of the location of S4, under the assumption of helical-screw motion, that indicates that the top S4 charges in the activated position are located ~11 Å from the center of the extracellular end of S5 (Fig. 5 *A*). It should be pointed out that, in our study, we do not obtain any information about the location of the intracellular end of S4. S4 could very well be tilted, and we have in Fig. 5 *B* suggested a possible three-dimensional location of S4.

The presented location of S4 deviates from recent suggestions. Studies based on tryptophan or alanine scanning, or energy-minimizing computer calculations tentatively locate S4 close to the interface between the subunits in voltage-gated potassium channels (Durell et al., 1998; Li-Smerin et al., 2000a,b; Hong and Miller, 2000). However, these investigations were not directly aimed at localizing S4 in relation to the pore.

Our calculation above was done with some simplistic assumptions: the exact positions of the side chains containing the charged groups, the local dielectric environment around the surface charges, and the position of S4 in the *z*-direction. However, calculations with reasonable variations of these assumptions show that the top charges of S4 are always located closer to the extracellular end of S5 than to S6 or the P helix (see Appendix). The calculations above were also done under the assumption of a helical-screw

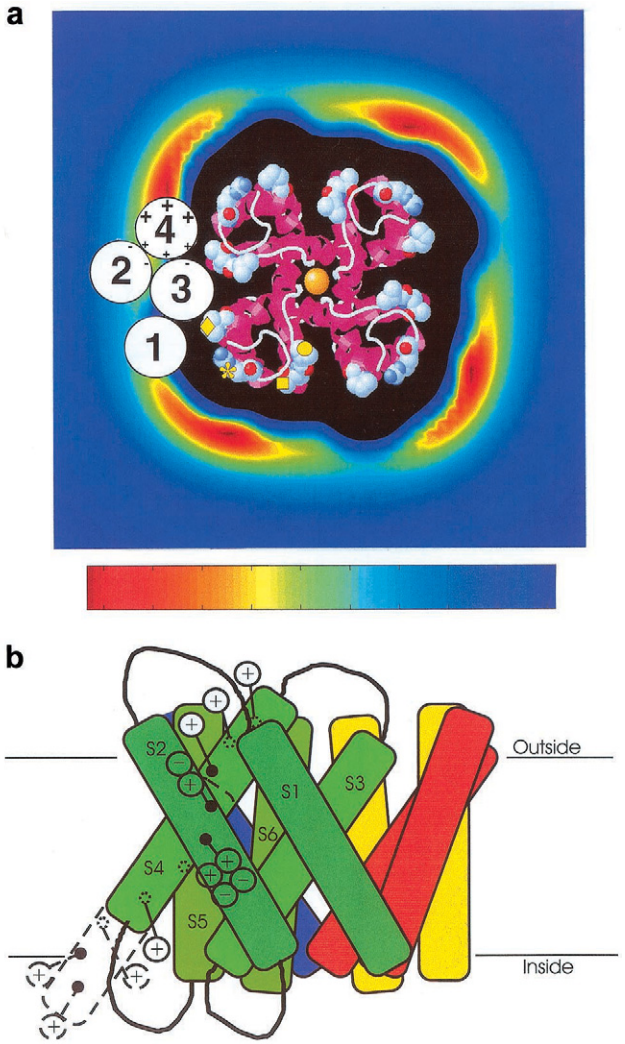

FIGURE 5 Structural models of a potassium channel. (*A*) Estimated location of the extracellular end of S4. Top view of the bacterial KcsA channel with r.m.s deviations between the experimental and theoretical surface potential values for different positions of S4 calculated with Eq. 5. The total area is 100 × 100 Å^2. The symbols (☆ for 419, ○ for 451, □ for 452, and ♦ for 430) mark the assumed positions of the charges (C_δ or the tip of the residue) used in the electrostatic calculations. The yellow circle in the center is a potassium ion in the selectivity filter. The color bar covers r.m.s. values from 0.77 to 5.60 mV. The black area in the center of the figure has an r.m.s. deviation ≫5.6 mV. The extracellular ends of the four S4 segments are most likely located in the dark red areas. In the upper left subunit, we have suggested positions of S1–S4 that are consistent with ours and other groups' experimental results (Tiwari-Woodruff et al., 1997; Baker et al., 1998; Li-Smerin et al., 2000a,b; Hong and Miller, 2000). The large + indicate the extracellular positions of the three top charges in the activated state. The small + indicate the positions of the intramembraneous charges. (*B*) Side view of the model in *A*. S5 and S6 from different subunits are shown in different colors (*red*, *yellow*, *blue*, and *green*). The proposed localization of S1–S4 in the green subunit is indicated. S4 is shown in both the resting (*dashed*) and the activated position.

motion of S4 (Catterall, 1986; Baker et al., 1998; Keynes and Elinder 1999). Other models of the S4 motion have also been suggested (Aggarwal and MacKinnon, 1996; Papazian

and Bezanilla, 1997; but see Horn, 2000). However, the fact that charges introduced in S5 have larger electrostatic effects than charges in other parts of the pore region suggests, for most models of S4 motion, that S4 is closest to S5.

In Fig. 5 we have, in addition to the position of S4, indicated tentative positions of the S1–S3 segments, based on experimental results from other studies (Tiwari-Woodruff et al., 1997; Baker et al., 1998; Li-Smerin et al., 2000a,b; Hong and Miller, 2000). The top S4 charges (R362, R365, and R368) are located in the extracellular solution (Baker et al., 1998), close to the red spot, while the S4 charges in the membrane (R371, K374, and R377) can make the interactions, with negative charges in S2 and S3, that were identified in intragenic suppression investigations (Tiwari-Woodruff et al., 1997). Large parts of S1 and S2 are facing the lipids, whereas S3 (placed in the groove between subunits) is mainly facing protein surfaces (Li-Smerin et al., 2000a; Hong and Miller, 2000). Finally, a portion of S5 is facing the lipids in contrast to the rest of the S5–S6 pore domain (Li-Smerin et al., 2000b). The suggested location of S4 would allow for large scale movements of S4 (e.g., helical screw motion) because one side (the hydrophobic side) of the transmembrane portion of the S4 helix would be facing the fluid lipid bilayer (Fig. 5). The main difference with the earlier work (e.g., Li-Smerin et al., 2000a,b) is that we place S3 at the center of the subunit instead of S4. Li-Smerin and coworkers mapped the residues of the pore region that is interacting with the voltage sensor module (i.e., S1–S4). In our model, this would suggest that it was S3's interaction surface with the pore region that was mapped in their work.

The present estimation of the location of S4 is important for future studies in determining the molecular coupling between the movement of the voltage sensor and the opening of the pore. It may also serve as guideline for future mapping of the outer segments S1, S2, and S3, as well as auxiliary β-subunits (Gulbis et al., 1999) in relation to the pore. Furthermore, the present method to determine structural features of the *Shaker* potassium channel can be used for other proteins where electrostatic effects are important.

APPENDIX: ERROR ESTIMATION IN S4 LOCATION

In the calculation in Fig. 5 *A*, we assumed that the three top S4 charges can be treated as a point charge. We have remade the calculation with the three charges placed as on an α-helix; each charge at the end of an arginine side chain in every third position of an α-helix (i.e., 60° between the residues when viewed along the central axis), and with the assumption that the total $G(V)$ shift is equal to the average surface charge effect on the three top S4 charges. The S4 helix was translated in the plane of the channel surface and rotated, in steps of 10°, around the z axis to reach the smallest r.m.s. deviation between the experimental $G(V)$ shifts (i.e., $\Delta\psi$) and the theoretical effects of the introduced surface charges on the S4 charges. The position of the center of the three charges that gave the smallest r.m.s deviation was within the bright red area in Fig. 5 *A* for every possible rotation of S4, indicting that our approximation of the three charges as a point charge does not greatly effect the result. The center of the S4 helix was always located <8 Å away from the hot spot in Fig. 5 *A*. The exact position of S4 depends also on the exact kinetic model for the opening/closing of the channels (i.e., which transition in the activation pathway causes the largest shift in the $G(V)$ for a change in the surface potential). However, the $G(V)$ shift is always smaller or equal to the change in surface potential at the most affected of the three top S4 charges. Therefore, it can be argued that the hotspot in Fig. 5 *A* is an upper limit of the distance between the surface charge and the nearest S4 charge, because, for any other assumption, at least one of the S4 charges has to be closer than this distance to get the experimentally observed $G(V)$ shift. This would move S4 closer to the pore region than in Fig. 5.

We identify four other possible sources of errors in our estimation of the location of S4, besides uncertainties in the exact model of the transmembrane motion of S4 discussed above:

1. For the locations of the introduced surface charges, we have used the positions indicated in Fig. 5 *A*. The positions of the side chains in *Shaker* are not necessarily the same as those in KscA. To estimate the sensitivity of our calculation to small changes in these positions, we made calculations where all charges, independent of each other, were moved up to 3 Å in all directions in the plane of the surface. The most likely position of S4 was still within the bright red area in Fig. 5 *A*.
2. The introduced surface charges are all located approximately in one plane (Fig. 1, *bottom*), but the position of the top S4 charges in the z-direction compared to this plane is unknown. In Fig. 5, we assumed that the top S4 charges are in this plane in the open state. We also made calculations in which the position of the top S4 charges was changed up to 12 Å in the z-direction compared to this plane. The effect of this change was that the hot spot moved closer to S5 in the x—y plane.
3. The absolute value of the electrostatic effect of charged residues at 430 was difficult to determine. We tested $\Delta\psi$ values between 0 and 6 mV for this position in the calculations. The corresponding change in the position of the minimum in Fig. 5 *A* was <1 Å.
4. To calculate the distance between S4 and a surface charge, we used Eq. 3, which is valid for charges on a flat surface at the border between a low-dielectric and a high-dielectric medium (McLaughlin, 1989). The channel surface is not flat, and the charges are not necessarily exactly located at the border (they may extend some Ångströms out in the extracellular solution). For a charge in free solution, one should use a Debye–Hückel–screened Coulomb potential, which is identical to Eq. 3 without the factor 2 in the numerator. We also did the calculations with this potential equation, which led to sharper minima moved toward 419 and the center of the channel by 4 Å.

We conclude that the position of the minimum indicated in Fig. 5 *A* is not sensitive to small changes in the assumptions of the calculation and (under the assumption of a helical-screw motion of S4) that the top S4 charges are located at this minimum, or even closer to S5.

We are grateful to Hans Elinder and Kristina Hasslund for some of the recordings, to Bo Rydqvist for comments on the manuscript, to Peter Löw for molecular enlightment, and to Carol Larsson and Russel Hill for editing the manuscript.

This work was supported by grants from the Swedish Medical Research Council (013043, 06552, 12554), Åke Wibergs Stiftelse, Magn. Bergvalls Stiftelse, The Swedish Society of Medicine, and Jeanssons Stiftelser.

F.E. and P.L. have junior research positions at the Swedish Medical Research Council.

REFERENCES

Aggarwal, S. K., and R. MacKinnon. 1996. Contribution of the S4 segment to gating charge in the *Shaker* K^+ channel. *Neuron.* 16:1169–1177.

Baker, O. S., H. P. Larsson, L. M. Mannuzzu, and E. Y. Isacoff. 1998. Three transmembrane conformations and sequence-dependent displacement of the S4 domain in *Shaker* K^+ channel gating. *Neuron.* 20: 1283–1294.

Catterall, W. A. 1986. Molecular properties of voltage-sensitive sodium channels. *Ann. Rev. Biochem*. 55:953–985.

Cha, A., G. E. Snyder, P. R. Selvin, and F. Bezanilla. 1999. Atomic scale movement of the voltage-sensing region in a potassium channel measured via spectroscopy. *Nature.* 402:809–813.

Doyle, D. A., J. M. Cabral, R. A. Pfuetzner, A. Kuo, J. M. Gulbis, S. L. Cohen, B. T. Chait, and R. MacKinnon. 1998. The structure of the potassium channel: molecular basis of K^+ conduction and selectivity. *Science.* 280:69–77.

Durell, S. R., Y. Hao, and H. R. Guy. 1998. Structural models of the transmembrane region of voltage-gated and other K^+ channels in open, closed, and inactivated conformations. *J. Struct. Biol.* 121:263–284.

Elinder, F., and P. Århem. 1998. The functional surface charge density of a fast K channel in the myelinated axon of *Xenopus laevis*. *J. Membrane Biol.* 165:175–181.

Elinder, F., and P. Århem. 1999. Role of individual surface charges of voltage-gated K channels. *Biophys. J.* 77:1358–1362.

Elinder, F., Y. Liu, and P. Århem. 1998. Divalent cation effects on the *Shaker* K channel suggest a pentapeptide sequence as determinant of functional surface charge density. *J. Membrane Biol.* 165:183–189.

Glauner, K. S., L. M. Manuzzu, C. S. Gandhi, and E. Y. Isacoff. 1999. Spectroscopic mapping of voltage sensor movement in the *Shaker* potassium channel. *Nature.* 402:813–817.

Grahame, D. C. 1947. The electrical double layer and the theory of electrocapillarity. *Chem. Rev.* 41:441–501.

Gulbis, J. M., S. Mann, and R. MacKinnon. 1999. Structure of the cytoplasmic β subunit-T1 assembly of voltage-dependent K^+ channels. *Cell.* 97:943–952.

Hille, B. 1992. Ionic Channels of Excitable Membranes. Sinauer Associates, Sunderland, MA. 457–470.

Hong, K. H., and C. Miller. 2000. The lipid–protein interface of a *Shaker* K^+ channel. *J. Gen. Physiol.* 115:51–58.

Horn, R. 2000. A new twist in the saga of charge movement in voltage-dependent ion channels. *Neuron.* 25:511–514.

Hoshi, T., W. N. Zagotta, and R. W. Aldrich. 1990. Biophysical and molecular mechanisms of *Shaker* potassium channel inactivation. *Science.* 250:533–538.

Kamb, A., L. E. Iversen, and M. A. Tanouye. 1987. Molecular characterization of *Shaker*, a *Drosophila* gene that encodes a potassium channel. *Cell.* 50:405–413.

Keynes, R. D., and F. Elinder. 1999. The screw-helical voltage gating of ion channels. *Proc. R. Soc. Lond. B.* 266:843–852.

Larsson, H. P., and F. Elinder. 2000. A conserved glutamate is important for slow inactivation in K^+ channels. *Neuron.* 27:573–583.

Larsson, H. P., O. S. Baker, D. S. Dhillon, and E. Y. Isacoff. 1996. Transmembrane movement of the *Shaker* K^+ channel S4. *Neuron.* 16:387–397.

Li-Smerin, Y., D. H. Hackos, and K. J. Swartz. 2000a. α-helical structural elements within the voltage-sensing domains of a K^+ channel. *J. Gen. Physiol.* 115:33–49.

Li-Smerin, Y., D. H. Hackos, and K. J. Swartz. 2000b. A localized interaction surface for voltage-sensing domains of a K^+ channel. *Neuron.* 25:411–423.

Mannuzzu, L. M., M. M. Moronne, and E. Y. Isacoff. 1996. Direct physical measure of conformational rearrangement underlying potassium channel gating. *Science.* 271:213–216.

Mathias, R. T., G. J. Baldo, K. Manivannan, and S. McLaughlin. 1992. Discrete charges on biological membranes. *In* Electrified Interfaces in Physics, Chemistry and Biology. R. Guidelli, editor. Kluwer Academic Publishers, Dordrecht, The Netherlands. 473–490.

McLaughlin, S. 1989. The electrostatic properties of membranes. *Ann. Rev. Biophys. Chem.* 18:113–136.

Papazian, D. M., and F. Bezanilla. 1997. How does an ion channel sense voltage? *News Physiol. Sci.* 12:203–210.

Peitzsch, R. M., M. Eisenberg, K. A. Sharp, and S. McLaughlin. 1995. Calculation of the electrostatic potential adjacent to model phospholipid bilayers. *Biophys. J.* 68:729–738.

Seoh, S. A., D. Sigg, D. M. Papazian, and F. Bezanilla. 1996. Voltage-sensing residues in the S2 and S4 segments of the *Shaker* K^+ channel. *Neuron.* 16:1159–1167.

Tiwari-Woodruff, S. K., C. T. Schulteis, A. F. Mock, and D. M. Papazian. 1997. Electrostatic interactions between transmembrane segments mediate folding of *Shaker* K^+ channel subunits *Biophys. J.* 72:1489–1500.

Tiwari-Woodruff, S. K., M.-c. A. Lin, C. T. Schulteis, and D. M. Papazian. 2000. Voltage-dependent structural interactions in the *Shaker* K^+ channel. *J. Gen. Physiol.* 115:123–138.

Yang, N., A. L. George, Jr., and R. Horn. 1997. Probing the outer vestibule of a sodium channel voltage sensor. *Biophys. J.* 73:2260–2268.

Yellen, G. 1998. The moving parts of voltage-gated ion channels. *Q. Rev. Biophys.* 31:239–295.

Yusaf, S. P., D. Wray, and A. Sivaprasadarao. 1996. Measurement of the movement of the S4 segment during the activation of a voltage-gated potassium channel. *Pflügers Arch*. 433:91–97.